Electronic structure and phase stability of disordered hexagonal close-packed alloys

Aftab Alam,[1] T. Saha-Dasgupta,[1] A. Mookerjee,[1] A. Chakrabarti,[1] and G. P. Das[2]
[1]*S. N. Bose National Centre for Basic Sciences, Kolkata 700098, India*
[2]*Indian Association for the Cultivation of Science, Jadavpur, Kolkata 700032, India*
(Received 11 December 2006; published 23 April 2007)

We report a systematic study of the electronic structure and phase stability of some of the hexagonal close-packed random binary alloys such as $Ru_{1-x}Re_x$, $Ti_{1-x}Zr_x$, $Rh_{1-x}Cr_x$, and $Ti_{1-x}Al_x$. First-principles calculations have been carried out using the augmented space recursion based on the tight-binding linear muffin-tin orbital basis. In particular, we have generalized our earlier applied augmented space recursive technique [T. Saha *et al.*, J. Phys.: Condens. Matter **6**, L245 (1995)] to the case of systems with more than one atom per unit cell, as is needed for hexagonal close-packed alloys. This involved development of a code that can handle any crystal structure with multiple sublattices. Ordering tendencies and phase stability are examined via effective pair interactions and their lattice Fourier transforms for TiAl alloy system, the low-temperature phase of which exhibits both face-centered cubic and hexagonal symmetry upon varying concentration. For each of the considered concentrations, the correct ordering tendency is obtained.

DOI: 10.1103/PhysRevB.75.134203 PACS number(s): 71.23.−k, 71.15.Mb, 71.20.Be

I. INTRODUCTION

In the recent past, there has been an increasing interest in the theoretical study of the electronic structure of hcp metals (see, e.g., Ref. 1, and references therein), and ordered intermetallics[2–4] using first-principles band-structure methods based on the local-density approximation (LDA). Typical methods used in these studies are the linear muffin-tin orbital (LMTO) method,[5] the pseudopotential treatment,[6] and the full-potential linear-augmented plane-wave approach.[7] On the other hand, the theoretical study of electronic structure of solid solutions of transition metals with the hcp structure is rather limited,[8–10] although these alloys have many interesting properties. The main reason behind this is the relatively complex structure of these materials with two atoms per unit cell as well as the deviation from the ideal c/a ratio imposing certain structural anisotropies. Some of these alloys are formed from constituents that themselves do not have the hcp crystal structure under the normal condition. This offers a possibility to study the electronic structure of these materials under varying structural conditions.

The purpose of the present paper is to present a first-principles electronic structure calculations of the hcp random transition metal alloys using the augmented space recursion (ASR),[11] combined with the tight-binding LMTO method. The ASR-LMTO technique has been developed over the years and has the important advantage of taking into account local environment effects such as off-diagonal disorder, lattice distortion,[12] and short-range order[13] in the formalism as compared to the coherent potential approximation (CPA)-based methods. The technique so far has been applied to only cubic alloy systems. In the present work, the technology has been generalized to handle any crystal structure with multiple sublattices, as is needed for hcp alloys. As case studies, we have chosen four hcp alloys, namely, $Ru_{1-x}Re_x$, $Ti_{1-x}Zr_x$, $Ti_{1-x}Al_x$, and $Rh_{1-x}Cr_x$. In the first two alloy systems, both the pure components crystallizes in the hcp structure. In the example of $Ti_{1-x}Al_x$, only one component (Ti) has the hcp structure. In the last example of $Rh_{1-x}Cr_x$, none of the pure components crystallizes in the hcp structure. In the latter two alloys, the hcp phase exists only over a limited concentration range. Such a choice allows us to make a systematic study of the electronic structure of disordered hcp alloys and also enables us to make a proper test of our formalism.

The other problem we would like to focus on is a first-principles study of the phase stability in this class of alloy systems. Alloy phase stability study, which involves determination of stability of the homogeneous disordered alloys with respect to concentration wave fluctuations using *ab initio* electronic structure calculations, is an important area of research. For this purpose, one needs a derivation of the configurational energy for the alloy system. Several methods,[14–16] with varying degrees of sophistication, have been proposed; in them the configurational energies are expressed in terms of effective multisite interactions, in particular, effective pair interactions.[17] In this paper, we have used a self-consistent ASR method coupled with the orbital peeling technique to compute the effective pair interactions. The ASR coupled with the orbital peeling technique[18] to evaluate small energy differences associated with band-structure energies have been successfully used in the past to describe the phase formation in alloys.[19] A scalar relativistic calculation of the electronic structure and phase stability analysis[20] has been also carried out. Using this approach, we have studied the phase stability of TiAl alloy system which crystallizes in hcp structure for certain concentration range. TiAl alloys are particularly interesting for their promising applications in the aerospace industry.[21] In addition to their excellent high-temperature properties, these alloys are light—about half as dense as Ni-based alloys which are traditionally used for aerospace applications. The equilibrium phases of $Ti_{1-x}Al_x$ alloys, for large concentrations of Al, are all formed in fcc-based structures. For the sake of completeness, we have therefore also carried out calculations in the fcc phase. To our knowledge, the present paper is perhaps one of the initial papers to deal with the phase stability of disordered hexagonal alloys from first principles. The earlier reported first-principle works in Refs. 8 and 9 on disordered hexagonal alloys involved calculations of only density of states, while

the work presented in Ref. 10 dealt with disordered hcp alloys and their thermodynamic properties such as formation enthalpy using special quasirandom structures.

The rest of the paper is organized as follows. In Sec. II, we shall describe in brief our theoretical framework for the electronic structure and phase stability calculations. Section III is devoted to describing the details of computations. The results of the density of states for $Ru_{1-x}Re_x$, $Ti_{1-x}Zr_x$, $Ti_{1-x}Al_x$, and $Rh_{1-x}Cr_x$ and the stability of ordered structures for the $Ti_{1-x}Al_x$ alloys will be discussed in Sec. IV. Finally, concluding remarks are drawn in Sec. V.

II. FORMALISM

The electronic structure of the hcp binary alloy $A_{1-x}B_x$ can be described by the most localized form of the second-order tight-binding (TB)-LMTO Hamiltonian,[5]

$$\mathbf{H} = \mathbf{H}^{(1)} - \mathbf{h}\ \mathbf{o}\ \mathbf{h},$$

$$\mathbf{H}^{(1)} = \sum_{R\alpha L} C_{R\alpha L}\mathbf{P}_{R\alpha L} + \sum_{R\alpha L}\sum_{R'\alpha' L'} \Delta^{1/2}_{R\alpha L} S_{R\alpha L,R'\alpha' L'} \Delta^{1/2}_{R'\alpha' L'} \mathbf{T}_{R\alpha L,R'\alpha' L'},$$

where

$$\mathbf{h} = \mathbf{H}^{(1)} - \sum_{R\alpha L} E^{(\nu)}_{R\alpha L}\mathbf{P}_{R\alpha L}$$

and

$$\mathbf{o} = \sum_{R\alpha L} O_{R\alpha L}\mathbf{P}_{R\alpha L}, \tag{1}$$

R and R' label the unit cell, α is the index of an atom within the hcp unit cell which can take value either 1 or 2 and L (ℓm) is the composite angular momentum index. The quantities C, Δ, and o are the potential parameters and are material dependent. S is the structure matrix which characterizes the hcp lattice geometry. $\mathbf{P}$ and $\mathbf{T}$ are the projection and transfer operators in the Hilbert space $\mathcal{H}$ spanned by the tight-binding basis $\{|R\alpha L\rangle\}$. For a disordered binary alloy A_xB_{1-x}, the potential parameters X $(=C,\Delta,o)$ can randomly take two different values $(X^A_L$ or $X^B_L)$ depending on whether the site R is occupied by an A atom or a B atom, so one can express X in terms of a random occupation variable (n_R) as

$$X_{RL} = X^A_L n_R + X^B_L(1-n_R),$$

where the random variable n_R can take a value of 1 if site R is occupied by an A atom with a probability x, otherwise 0 with probability $(1-x)$.

In an earlier work,[11] we described in detail how to perform the configurational averaging of the resolvent $\mathbf{G}(z) = (z\mathbf{I}-\mathbf{H})^{-1}$ within the ASR. There we studied a cubic lattice, but the same method with generalization can be applied to hcp with two equivalent atoms per unit cell. Below, we briefly mention the salient points of ASR.

The basic idea behind the augmented space formalism is to borrow an idea from measurement theory and associate with each random variable n_R an operator $\mathbf{M}_R$ such that the probability density of the random variable is the spectral density of $\mathbf{M}_R$. These operators act on the configuration space Φ of the variables $\{n_R\}$. For a set of binary variables, this space is isomorphic to the configuration space of a spin-(1/2) Ising model. If we now construct an augmented Hamiltonian $\tilde{\mathbf{H}}$ in the space $\Omega = \mathcal{H}\otimes\Phi$ by replacing every random variable by its associated operator, the augmented space theorem[22] states that the configuration average of any functional of the random Hamiltonian is a specific matrix element of the same functional of the augmented Hamiltonian in Ω.

For a binary alloy A_xB_{1-x}, the configuration space of a single occupation variable is spanned by $|\uparrow_R\rangle = \sqrt{x}|A\rangle + \sqrt{1-x}|B\rangle$ and $|\downarrow_R\rangle = \sqrt{1-x}|A\rangle - \sqrt{x}|B\rangle$

$$n_R \rightarrow \mathbf{M}_R = x\mathbf{P}^{\uparrow}_R + (1-x)\mathbf{P}^{\downarrow}_R + \sqrt{x(1-x)}(\mathbf{T}^{\uparrow\downarrow}_R + \mathbf{T}^{\downarrow\uparrow}_R),$$

where $\mathbf{P}_R$ and $\mathbf{T}_R$ are the projection and transfer operators in the configuration space Φ.

The configuration average of the Green function, for example, is then

$$\langle\langle \mathbf{G}(z)\rangle\rangle_{R\alpha L,R'\alpha' L'} = \bar{G}(z)_{R\alpha L,R'\alpha' L'} = \langle\{\varnothing\}\otimes R\alpha L|(z\tilde{\mathbf{I}}-\tilde{\mathbf{H}})^{-1}|\{\varnothing\}\otimes R'\alpha' L'\rangle, \tag{2}$$

where $\{\varnothing\} = \{\uparrow\uparrow\cdots\uparrow\}$ is a state in configuration space Φ. We may notice that in the present theoretical framework, the configuration averaging of a quantity simply reduces to the evaluation of a particular matrix element in the enlarged augmented space Ω. This theoretical result is *exact*. The actual numerical implementation is then carried out using the recursion method of Haydock *et al.*[23] which produces a continued fraction expansion for the diagonal part of the configuration-averaged Green function,

$$\bar{G}(z)_{R\alpha L,R\alpha L} = \cfrac{1}{z-a_1-\cfrac{b_1^2}{z-a_2-\cfrac{b_2^2}{z-a_3-\cfrac{b_3^2}{\cdots}}}}.$$

Proper termination of the asymptotic part of this continued fraction constitutes the only approximation in the present theory. This termination must retain the essential Herglotz analytic properties of the Green function. Haydock[23] carried out extensive studies of the errors involved and precise estimates are available in the literature. Several terminators are available and we have chosen to use that of Beer and Pettifor.[24] If one calculates the coefficients up to the nth step exactly, the first $2n$ moments of the density of states are reproduced exactly. The terminator is chosen so that the asymptotic moments are also accurately reproduced. This is a generalization of the method of moments, with the additional restriction that the asymptotically large moments are also accurately obtained.

For the phase stability study, we start from a completely disordered alloy with each site R having an occupation variable n_R associated with it. In this homogeneously disordered background we introduce fluctuations in the occupation variable at each site: $\delta x_R = n_R - x$. The total energy in this configuration $\{\sigma\}$ can then be expanded about the energy of the perfectly disordered state as

$$E(x) = E^{(0)} + \sum_{R=1}^{N} E_R^{(1)} \delta x_R + \sum_{RR'=1}^{N} E_{RR'}^{(2)} \delta x_R \delta x_{R'} + \cdots, \quad (3)$$

where $E^{(0)}$ is the energy of the averaged disordered medium. $E_R^{(1)}$, though concentration- and temperature-dependent but structure insensitive, should not be considered in the stability analysis. The pair interactions $E_{RR'}^{(2)}$ express the correlation between two sites and are the most dominant quantities for the analysis of phase stability.

If we embed atoms of type A or B at site R in the disordered background and the total energies are E_R^A and E_R^B, then by the above equation,

$$E_R^{(1)} = E_R^A - E_R^B.$$

This is one-body interaction resulting from the interchange of a B atom with an A atom at site R in the alloy. Similarly, $E_{RR'}^{(2)}$ is the pair interaction, which is the difference in the one-body interactions at R when site $R'(\neq R)$ is occupied either by an A or a B atom

$$E_{RR'}^{(2)} = E_{RR'}^{AA} + E_{RR'}^{BB} - E_{RR'}^{AB} - E_{RR'}^{BA}.$$

$E_{RR'}^{\alpha\beta}$ is the energy of random AB alloy with sites R and R' occupied by α and β types of atoms. Brute force method for the calculation of $E_{RR'}^{(2)}$ involves error due to subtraction of large numbers. To avoid such error, instead we follow the alternative route described below.

The total energy of a solid consists of two parts: a one electron band contribution E_{BS} and the electrostatic contribution E_{ES}. The cluster interactions defined in Eq. (3), in principle, include both E_{BS} and E_{ES} contributions. However, since the cluster interactions involve the difference of cluster energies, the electrostatic terms may be assumed to cancel out, considering only the band-structure contribution to be important. Such an assumption, though not rigorously true, has been shown to hold good in a number of alloy systems.[25] If we consider only the band-structure contribution, the effective pair interactions may be written as[20]

$$E_{RR'}^{(2)} = -\int_{-\infty}^{E_F} dE \left(-\frac{1}{\pi} \Im m \left\{ \log \sum_{IJ} \det[G^{IJ}(E)] \right\} \zeta_{IJ} \right), \quad (4)$$

where G^{IJ} represents the configurationally averaged Green function corresponding to the disordered Hamiltonian, whose R and R' sites are occupied by Ith and Jth types of atom, and

$$\zeta_{IJ} = \begin{cases} +1 & \text{if } I = J \\ -1 & \text{if } I \neq J. \end{cases}$$

The behavior of this function is quite complicated and hence the integration by standard routines is difficult, involving many iterations before convergence is achieved. Furthermore, the integrand is multivalued, being simply the phase of $\Sigma_{IJ} \det(G^{IJ}) \zeta_{IJ}$. The way out for this was suggested by Burke[18] and relies on the repeated application of the partition theorem on the Hamiltonian $\tilde{\mathcal{H}}^{IJ}$. The final result is given in terms of the zeros and poles of the Green function in the region $E < E_F$,

$$E_{RR'}^{(2)} = 2 \sum_{IJ} \zeta_{IJ} \sum_{k=0}^{l_{max}} \left[\sum_{j=1}^{z^{k,IJ}} Z_j^{k,IJ} - \sum_{j=1}^{p^{k,IJ}} P_j^{k,IJ} + (p^{k,IJ} - z^{k,IJ}) E_F \right], \quad (5)$$

where $Z_j^{k,IJ}$ and $P_j^{k,IJ}$ are the zeros and poles of the configuration averaged, peeled Green function G_k^{IJ} of the disordered Hamiltonian with occupancy at sites R and R' by I and J types of atoms, of which the $(k-1)$ rows and columns have been deleted. $p^{k,IJ}$ and $z^{k,IJ}$ are the number of poles and zeros in the energy region below E_F.

The augmented space recursion method using first-order TB-LMTO Hamiltonian to calculate the configuration averaged, peeled Green function has been described in an earlier paper.[20] A similar procedure can be applied for the case of a second-order TB-LMTO Hamiltonian [Eq. (1)], as used in the present calculations, giving rise to more accurate results. We refer the reader to this earlier paper and the references therein for the details.

The symmetry properties of the pair interactions, $E_{RR'}^{(2)} \equiv V_{RR'}$ can be used to explain a wide range of phenomena related to order-disorder transitions.[26] Analysis can be made in terms of $V(h)$ which is the Fourier transformation of $V_{RR'}$ evaluated at a specific point h in the $\mathbf{k}$ space. If a symmetry element of the space group is located at a point h, the vector representing the gradient $\nabla_h V(h)$ of an arbitrary potential-energy function $V(h)$ at that point must lie along or within the symmetry element. If two or more symmetry elements intersect at point h, one must necessarily have

$$|\nabla_h V(h)| = 0, \quad (6)$$

since a finite magnitude vector cannot lie simultaneously on intersecting straight lines having only a point in common. At these so-called special points, the potential-energy function $V(h)$ represents a minimum. Thus, special points play an important role in the search for lowest-energy-ordered structures. These special points are always located at the surface of the Brillouin zone (BZ). The *star* of a special point vector $\mathbf{k}$ is obtained by applying all the rotations and rotation inversions of the space group on the vector $\mathbf{k}$. All these vectors of a star are considered equivalent. The special points of the fcc structure are located at the points Γ, X, W, and L of the Brillouin zone, as listed in Table I. There are four special points in this case predicting various kinds of ordered structures (as shown in the last column) that could be obtained by the superposition of concentration waves for equivalent points corresponding to a single star.

In the case of the hcp structure, we have two atoms per unit cell; furthermore, the space group of the structure $P6_3/mmc$ (or D_{6h}^4) is not symmorphic and hence the analysis is more subtle. With 1 and 2 denoting the two simple hex-

TABLE I. Relevant special points and corresponding stars of the fcc and hcp lattices. The rightmost column shows the respective BZs.

	Star	Members of the star	BZ points	Ordered structure	
fcc	<000>	[000]	Γ	Phase segregation	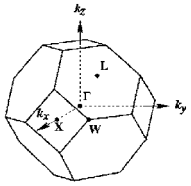
	<100>	[100] [010] [001]	X	$L1_0$, Ll_2	
	<1 1/2 0>	[1 1/2 0] [1/2 0 1] [0 1 1/2] [$\bar{1}$ $\bar{1}$/2 0] [1/$\bar{2}$ 0 $\bar{1}$] [0 $\bar{1}$ $\bar{1}$/2]	W	DO_{22}, A_2B_2	
	<1/2 1/2 1/2>	[1/2 1/2 1/2] [1/2 $\bar{1}$/2 $\bar{1}$/2] [$\bar{1}$/2 1/2 $\bar{1}$/2] [$\bar{1}$/2 $\bar{1}$/2 1/2]	L	$L1_1$	
hcp	<000>	[000]	Γ	Phase segregation	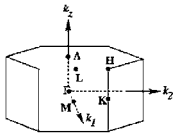
	<1/2 0 0>	[1/2 0 0] [0 $\bar{1}$/2 0] [$\bar{1}$/2 1/2 0]	M	CuPt like B_{19},DO_{19}	
	<1/3 1/3 1/2>	[1/3 1/3 1/2] [$\bar{1}$/3 $\bar{1}$/3 1/2]	H	No structure	

agonal sublattices, one needs two kinds of concentration waves p_k^1 and p_k^2

$$p_k^{1(2)} = \frac{1}{N_c} \sum_{\mathbf{n} \in 1(2)} e^{i\mathbf{k}.\mathbf{n}} p_{\mathbf{n}}, \tag{7}$$

where $N_c (=\frac{1}{2}N_a)$ is the number of unit cells. The sum over the vectors $\mathbf{n}$ are always vectors of the hexagonal Bravais lattice. One can now define the Fourier transforms of the pair interactions $V_{\alpha\beta}(\mathbf{k})$, where $\alpha, \beta = 1, 2$ corresponding to two sublattices in the hexagonal lattice

$$V_{11}(\mathbf{k}) = V_{22}(\mathbf{k}) = \sum_{\mathbf{n}} V(\mathbf{n}) e^{i\mathbf{k}.\mathbf{n}},$$

$$V_{12}(\mathbf{k}) = V_{21}^*(\mathbf{k}) = \sum_{\mathbf{n}} V(\mathbf{n} + \tau) e^{i\mathbf{k}.\mathbf{n}}, \tag{8}$$

$\boldsymbol{\tau}$ is the vector $\left[\frac{2}{3}\frac{1}{3}\frac{1}{2}\right]$ joining the two atoms of the elementary cell and $V(\mathbf{n})$ is the nth neighboring pair interaction energies. In order to minimize the energy, we must diagonalize $V_{\alpha\beta}(\mathbf{k})$. This yields the two eigenvalues $V(\mathbf{k}) = V_{11}(\mathbf{k}) \pm |V_{12}(\mathbf{k})|$. There are six special points for a simple hexagonal structure; however, some of them are irrelevant for the analysis of ordered of structure. The relevant special points for a hcp structure are given in Table I.

Since there are two extrema at the special points, such as Γ and M, we must combine the concentration waves in the two sublattices in two different ways. These combinations are obtained from the eigenvectors of the matrix $V_{\alpha\beta}(\mathbf{k})$. The result is that at Γ and M, we have the simple modes $p_k^1 \pm p_k^2$, which may be called acoustic and optical modes. The acoustic mode $\langle 000 \rangle_I$ corresponds to a segregation process, whereas the optical mode $\langle 000 \rangle_{II}$ corresponds to an alternate stacking of pure A and B triangular planes. There can be three possible structures corresponding to the star M. These are CuPt-like structure, $B19$ (MgCd-like), and DO_{19} structure. There is no real structure associated with the star H $\left\langle \frac{1}{3}\frac{1}{3}\frac{1}{2} \right\rangle$, while some superstructure is formed that is related rather to a nonspecial point. For further details, we refer the reader to the article in Ref. 27.

III. COMPUTATIONAL DETAILS

In the TB-LMTO-ASR method, the difficulties are associated with the large rank of the enlarged augmented space. The rank of this Hilbert space is $N \times 2^N$ for a system of N lattice sites with binary distribution. In an earlier communication,[28] we have discussed how one may use the local symmetries of the augmented space to reduce the rank of the Hamiltonian and carry out the recursion on a reducible subspace of much lower rank. In the case of pair interaction calculation, if we fix the occupation of two sites (Ith and Jth sites), the local symmetry of the augmented space is further lowered. We may then carry out the recursion in a suitably reduced space.

For our calculations, the real-space clusters were generated out of 1200–1500 atoms, which gave rise to about 200 000 sites in the enlarged full augmented space, consisting of both real space and configuration space. After symmetry reduction, the number of sites in the reduced space becomes $\approx$10 000 leading to a significant reduction in computational cost. Twelve steps of recursion were carried out attached with a terminator by Beer and Pettifor[24] to construct the configuration-averaged Green function.

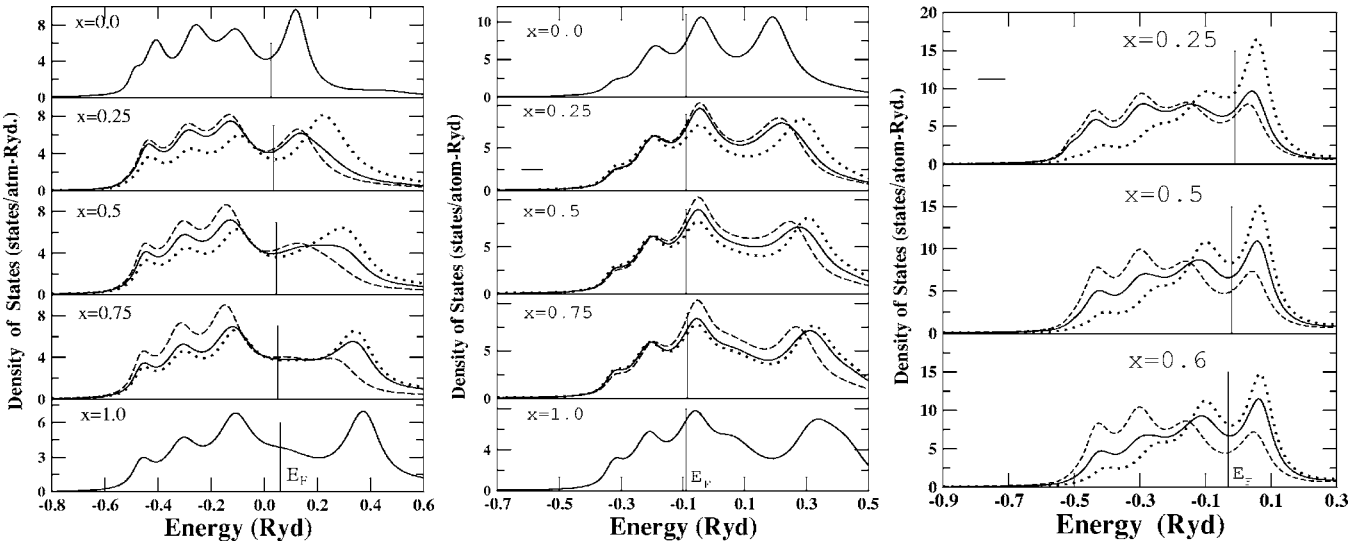

FIG. 1. Density of states for the three alloy systems $Ru_{1-x}Re_x$ (left panel), $Ti_{1-x}Zr_x$ (middle panel), and $Rh_{1-x}Cr_x$ (right panel). The last alloy system remains in the hcp structure in the concentration range $0.25 \leqslant x \leqslant 0.60$. The dashed and dotted lines indicate the *d*-projected density of states on the *A* atom and *B* atom, respectively, for the $A_{1-x}B_x$ alloy. The black solid line indicates the total density of states. The alloy Fermi levels E_F are indicated by the vertical lines in each panel.

We have calculated the effective pair potentials at the Fermi level so there is a need for very careful determination and convergence of the Fermi level. To determine the Fermi energy, we have carried out the calculations using energy-dependent formulation of augmented space recursion in which the disordered Hamiltonian with diagonal as well as off-diagonal disorder is recast into an energy-dependent Hamiltonian having only diagonal disorder. This allows one to sample more shells in the augmented space, in which the full real-space map is collapsed using lattice translation symmetry in augmented space. This formulation reduces the computational cost considerably; as an example, a real-space-based augmented space map with size of 250 000 becomes 5000 in the *k*-space-based-augmented space map. However, in this formulation the recursion becomes energy dependent and it is not suitable to carry out recursion for each energy point. This is tackled by choosing a few seed points across the energy spectrum uniformly and then carrying out recursion on those points and spline fitting the coefficients of recursion throughout the whole spectrum.[29] This enabled us to carry out large number of recursion steps since the configuration space grows significantly less faster for diagonal as compared to off-diagonal disorder. Using this formulation, we have checked the convergence of Fermi energy.

The calculation of Madelung potential is a challenging job for disordered alloys due to the absence of lattice periodicity. For the proper treatment of the Madelung potential, we have used the recently developed fully self-consistent TB-LMTO-ASR calculation[30] which correctly takes into account the charge neutrality and total-energy convergence.

IV. RESULTS AND DISCUSSION

For the application of our formalism, we have considered three characteristic set of examples. The first set of example consists of $Ru_{1-x}Re_x$ and $Ti_{1-x}Zr_x$ where the pure constituents in both the cases crystallizes in hcp structure. The second set of example is $Ti_{1-x}Al_x$ where only one constituent crystallizes in hcp structure and the other constituent crystallizes in fcc structure. The third example is $Rh_{1-x}Cr_x$ where none of the pure constituents crystallizes in the hcp structure. For all of these examples, we have calculated the density of states and compare our results with the earlier available data, and hence examined the effectiveness of TB-LMTO-ASR method to describe the electronic structure of disordered hcp alloys. We have then concentrated on the phase stability of a particular alloy, namely, $Ti_{1-x}Al_x$, for which extensive amount of experimental and theoretical results are available in the literature.[31] All calculations were performed with scalar relativistic LDA Hamiltonian.

In all systems investigated here, the c/a ratio remains essentially unchanged with varying concentration; it is about 1.599 in $Ru_{1-x}Re_x$,[8] 1.585 in $Ti_{1-x}Zr_x$, 1.598 in $Rh_{1-x}Cr_x$,[9] and about 0.802 77 in $Ti_{1-x}Al_x$ (Ref. 32) alloys over the concentration range where the hcp phase exists. The equilibrium lattice parameters are given by $a=2.73$ Å and $c=4.365$ Å for $Ru_{1-x}Re_x$, $a=3.09$ Å and $c=4.898$ Å for $Ti_{1-x}Zr_x$, $a=2.6785$ Å and $c=4.2816$ Å for $Rh_{1-x}Cr_x$, and $a=5.78$ Å and $c=4.64$ Å for hcp $Ti_{75}Al_{25}$. For fcc-based TiAl alloys, it is $a=3.991$ Å. The equilibrium lattice parameters are obtained by minimizing the total energies of the disordered alloys with respect to the lattice parameters.

A. Electronic structure of hcp alloys

Figure 1 shows the density of states for the three alloy systems, namely, $Ru_{1-x}Re_x$, $Ti_{1-x}Zr_x$, and $Rh_{1-x}Cr_x$. While the hcp $Ru_{1-x}Re_x$ and $Ti_{1-x}Zr_x$ exist in the whole concentration range, the hcp region of $Rh_{1-x}Cr_x$ alloy is limited ($0.25 \leqslant x \leqslant 0.60$). All the calculations have been carried out for concentrations $x=0.0$, 0.25, 0.5, 0.75, and 1.0, with the

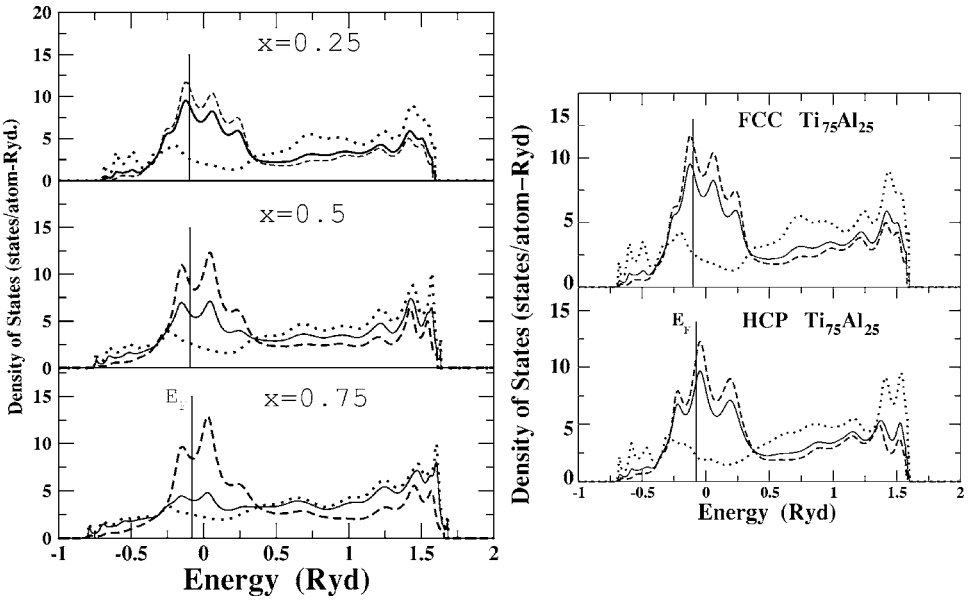

FIG. 2. Density of states for $Ti_{1-x}Al_x$ alloy. The left panel indicates the result for this alloy in the fcc structure. The panel in the right compares the density of states for $Ti_{75}Al_{25}$ alloy in the fcc and hcp structures. The different curves in each panel have the same meaning as that of Fig. 1. The alloy Fermi levels E_F are indicated by the vertical lines.

exception of $Rh_{1-x}Cr_x$, for which only concentrations $x=0.25$, 0.5, and 0.6 have been considered. The figure shows only the *d*-projected density of states, the solid line of which indicates the total density of states (DOS) of $A_{1-x}B_x$ alloy, the dashed line indicates the DOS on the first atom (A), and the dotted line indicates the same quantity but on the second atom (B). We have chosen to show only the *d*-projected density of states to compare with previously published results.[8,9] In all the panels, the alloy Fermi level E_F is indicated by the vertical line.

Starting from the leftmost column for $Ru_{1-x}Re_x$ alloys, we notice that the Fermi energy lies more or less in the middle of total *d*-bandwidth since both Ru and Re are located in the middle of the transition-metal series. The unoccupied states above E_F in the random alloys are influenced by disorder more significantly than occupied states below E_F. We also notice an increase in the alloy bandwidth with increasing Re content, which happens due to larger bandwidth of Re, which is a 5*d* element compared to Ru which is a 4*d* element. The Fermi level shifts slightly with concentration, as the number of valence electrons changes by only one in moving from Ru to Re. Overall agreement with the TB-LMTO-CPA result by Kudrnovsky *et al.*[8] is observed.

Focusing on the $Ti_{1-x}Zr_x$ results, it is evident that the total DOS of occupied states below $E \simeq 0$ Ryd changes extremely weakly with the alloy concentration. In the regime of unoccupied states, one can see a gradual transformation of a narrow *d*-band peak $E \simeq 0.2$ Ryd (for Ti) to a broader *d* peak situated at $E \simeq 0.33$ Ryd (For Zr *d* states). In this case, however, the Fermi level E_F essentially remains unchanged on alloying because the Ti and Zr atoms have the same number of valence electrons.

The rightmost panel shows the results for the $Rh_{1-x}Cr_x$ alloys. Though none of the pure components of this alloy has the hcp structure, the alloy maintains the hcp structure over a limited concentration range $0.25 < x < 0.6$. Unlike the previous two cases, the density of states in this case has very different characteristic features. The lower-energy states are predominantly Rh-like, while those around and above $E=0$ Ryd are mostly Cr-like. This indicates a strong influence of diagonal disorder. Similar kind of behavior has also been observed in the TB-LMTO-CPA results.[9]

B. Electronic structure and phase stability of $Ti_{1-x}Al_x$

Having established the feasibility and accuracy of augmented space recursion for disordered hcp alloys in general, we now focus on the alloy system of our interest, namely, $Ti_{1-x}Al_x$. We carry out the density of states as well as the phase stability study of this alloy system. As mentioned already, the low-temperature phases of $Ti_{1-x}Al_x$ show both fcc and hcp symmetries. The low Al content regime of $Ti_{75}Al_{25}$ forms in hcp symmetry. In Fig. 2 we show the density of states of $Ti_{1-x}Al_x$ alloy for $x=0.25$, 0.5, and 0.75. The underlying symmetry has been assumed to be fcc. The right panel of Fig. 2 compares the result for $x=0.25$ with computed DOS of correct hcp symmetry. Compared to the previous plots in Fig. 1, the plotted density of states here includes all of *spd* contributions. Comparing the fcc and hcp DOSs of $Ti_{75}Al_{25}$ alloy, we notice that the overall qualitative feature is not very different in the two structures. The Fermi energy also lies almost at the same level in the two cases. This is not unlikely since with only first nearest-neighbor interactions and the tetrahedron approximation in fcc lattice, the hcp-disordered phase α is equivalent to the fcc-disordered phase δ.[33] For ordered compounds, the fcc-based structures and the corresponding hcp-based structures are also found to have similar enthalpies of formation.[34]

We now discuss in the following the phase stability study of $Ti_{1-x}Al_x$ alloys. In order to correctly predict the types of ordering in various disordered alloys, we have computed the pair potential function $V(\mathbf{k})$ in the reciprocal space representation, which can be calculated from the Fourier transform of the real-space pair interaction energies $V_{RR'}$, where R and R' belong to either first, second, or third, or fourth neighbor shell.

In Fig. 3 we have shown the effective pair interaction for three TiAl alloys with the fcc structure. The studies have

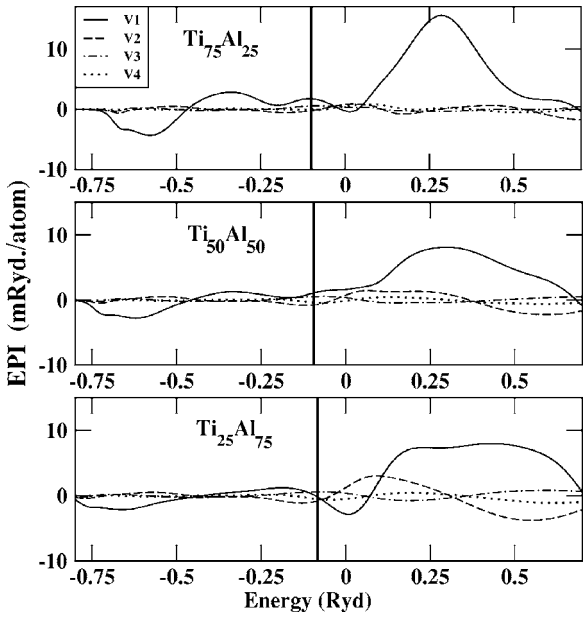

FIG. 3. The real-space effective pair interactions plotted as a function of energy for three TiAl alloys: $Ti_{75}Al_{25}$, $Ti_{50}Al_{50}$, and $Ti_{25}Al_{75}$. The solid, dashed, dot-dashed, and dotted lines in all the three panels indicate the pair interaction energies between the first (V_1), second (V_2), third (V_3), and fourth (V_4) neighboring atoms. The vertical line indicates the alloy Fermi level.

been made for $x=0.25$, 0.5, and 0.75. Although for $x=0.25$, the underlying crystal structure in reality is hcp, it is interesting to study the case of fcc to know what would have been the ordered structure if the alloy happened to continue in fcc phase. This is of interest since the hcp phase diagram is predicted to be similar to fcc phase diagram and may be obtained by replacing the fcc-based $L1_2$ and $L1_0$ by the hcp-based phases DO_{19}, and $B19$, respectively.[33] The solid, dashed, dot-dashed, and dotted lines show the pair interaction energies between the first (V_1), second (V_2), third (V_3), and fourth (V_4) nearest-neighboring atoms. A careful inspection of these data indicates that the magnitude of the pair interaction energy between the first neighboring atom (V_1) is always greater than the other pair energies (V_2, V_3, and V_4). Also, V_1 is always +ve which predicts an ordering behavior in all the three alloys. One, however, also needs to know the type of ordering. In the case of fcc lattice, one can have four types of possible ordered structures depending on the composition of the alloy. These are $L1_2$, DO_{22}, $L1_0$, and A_2B_2. Figure 4 shows the effective pair potential function in $k_z=0$ plane for the TiAl alloys in the fcc structure. Each of these plots has a minima at the special point [100] which correctly predicts the stability of $L1_2$ structure for $Ti_{75}Al_{25}$ and $Ti_{25}Al_{75}$ alloys and the stability of $L1_0$ structure for $Ti_{50}Al_{50}$ alloy. The quantitative estimates of V_{min} for each case have been listed in Table II. Another way of predicting the stability of these ordered structures is to calculate and check the sign of the antiphase boundary (APB) energy. The APB energy is the difference in the ordering energy between two competing superstructures such as $L1_2$ and DO_{22} or $L1_0$ and A_2B_2 defined as $\xi=-V_2+4V_3-4V_4$. This is the energy associated with $\frac{1}{2}[110]$ displacement between two [001] planes in

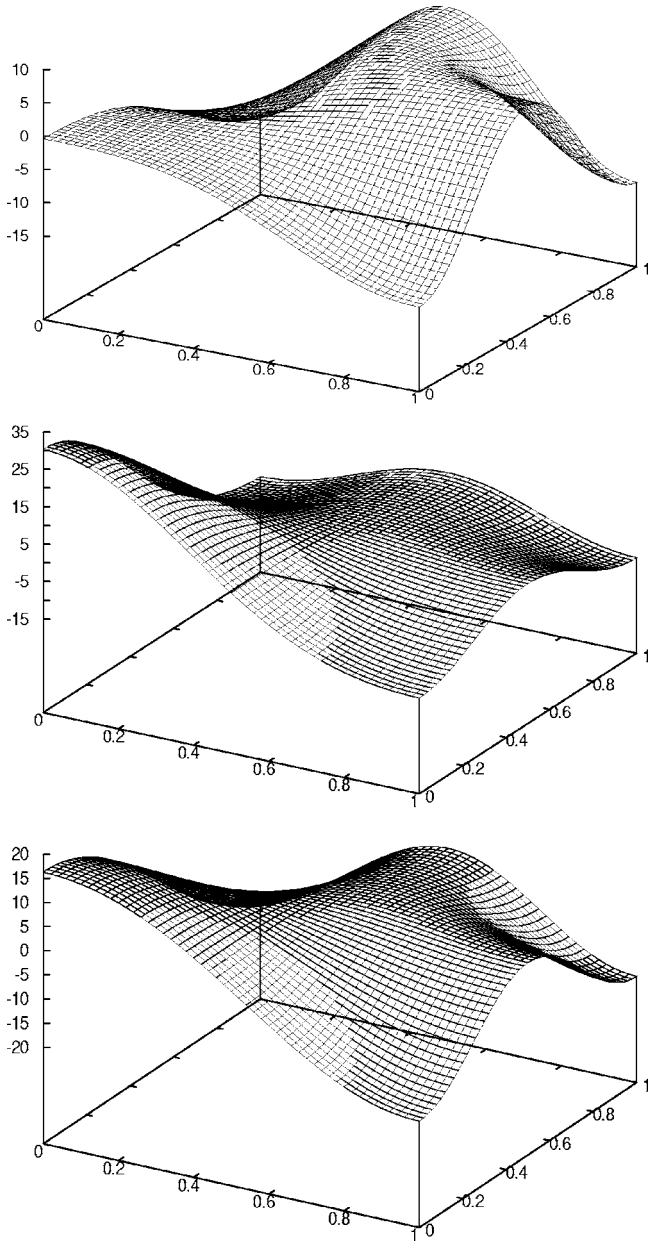

FIG. 4. The effective potential function $V(\mathbf{k})$ in the reciprocal space in the $k_z=0$ plane for the $Ti_{75}Al_{25}$ (top panel), $Ti_{50}Al_{50}$ (middle panel), and $Ti_{25}Al_{75}$ (bottom panel) alloys.

a fcc lattice. In Table III we have quoted the antiphase boundary energies for the three fcc $Ti_{1-x}Al_x$ alloys. The +ve sign of antiphase boundary energy at all three concentrations

TABLE II. Minima of the effective pair potential $V(\mathbf{k})$ for fcc- and hcp-based $Ti_{1-x}Al_x$ alloys.

Alloy system	Experimental ordering	$V_{\{min\}}$
fcc $Ti_{75}Al_{25}$	$\langle 100\rangle L1_2$	−14.81
fcc $Ti_{50}Al_{50}$	$\langle 100\rangle L1_0$	−17.97
fcc $Ti_{25}Al_{75}$	$\langle 100\rangle L1_2$	−14.40
hcp $Ti_{75}Al_{25}$	$\langle \frac{1}{2}00\rangle DO_{19}$	−43.64

TABLE III. APB energy (mRyd/atom) for three fcc $Ti_{1-x}Al_x$ alloys. The second column indicates the type of ordering taking place in respective cases.

Alloy system	Type of ordering	APB energy
fcc $Ti_{75}Al_{25}$ alloy	$L1_2$	2.94
fcc $Ti_{50}Al_{50}$ alloy	$L1_0$	4.45
fcc $Ti_{25}Al_{75}$ alloy	$L1_2$	5.21

predicts the stability of $L1_2$ structure both at $x=0.25$ and $x=0.75$ and the stability of $L1_0$ structure at $x=0.5$ concentration for $Ti_{1-x}Al_x$ alloy.

We have then investigated the most stable ordered structure in the case of hcp $Ti_{75}Al_{25}$ alloy. Unlike the fcc case, here one has two distinct types of real-space pair interaction energies, namely, V_{11} $(=V_{22})$ and V_{12} $(=V_{21})$. $V_{\alpha\alpha}$ is pair interaction between two atoms, both of which belongs to equivalent sublattices (α), and $V_{\alpha\beta}$ is the pair interaction between two atoms, one of which belongs to the sublattice α and the other to a different sublattice β. To be precise, one has to fix the origins in each sublattice and then proceed to do the calculations. This leads to 2×2 matrix form of the Fourier transform of the pair interaction $V_{\alpha\beta}(\mathbf{k})$, with α, $\beta=1,2$. The top panel of Fig. 5 shows the matrix elements $V_{11}^{(n)}$ and $V_{12}^{(n)}$ till second nearest neighbor, i.e., $n=1,2$. To minimize the pair interaction energy, one needs to diagonalize the matrix $V_{\alpha\beta}(\mathbf{k})$, which yields two eigenvalues $V^{\pm}(\mathbf{k})=V_{11}(\mathbf{k})\pm V_{12}(\mathbf{k})$. One of these pair potential surfaces $[V^{+}(\mathbf{k})]$ corresponds to an acoustic mode and the other $[V^{-}(\mathbf{k})]$ to an optical mode. There can be various superordered structures associated with the acoustic mode; however, there exists no structure corresponding to the optical mode. We have plotted the pair potential surface $V^{+}(\mathbf{k})$ in the bottom panel of Fig. 5. This plot shows a minima at the special point $[\frac{1}{2}00]$. Such a minima in the case of hcp alloys $A_{1-x}B_x$ with concentration $x=0.25$ can be related to the stability of DO_{19} structure.

Once the effective pair potential surface is calculated and the minima are located, the instability temperature T_0 can be calculated from the relation

$$\beta_0 x(1-x)V_{\{min\}}=1, \tag{9}$$

where $\beta_0=1/kT_0$. Employing the $V_{\{min\}}$ listed in Table II and plugging in Eq. (9) give the instability temperature as $\approx$1300 K, which is in reasonable agreement with the experimental measured order-disorder transition temperature of 1453 K.

V. CONCLUSION

Employing augmented space recursion in TB-LMTO basis, we studied the electronic structure of hcp-based disordered alloys. We have applied the developed technique to RuRe, TiZr, RhCr, and TiAl alloy systems. Good agreement with previously published results is obtained for RuRe, TiZr, and RhCr alloy systems. We further extended our theory to studying the problem of phase stability in hcp-based alloys by combining ASR with orbital peeling technique. The applicability of the theory is proved by considering TiAl alloy system which is of significant technological importance. Our predicted ordered structure is in conformity with experiment and the computed instability temperature is also in good agreement with experimentally measured order-disorder transition temperature. For the sake of completeness, we have also investigated fcc-based TiAl alloy system which occurs in Al-rich part of the phase diagram.

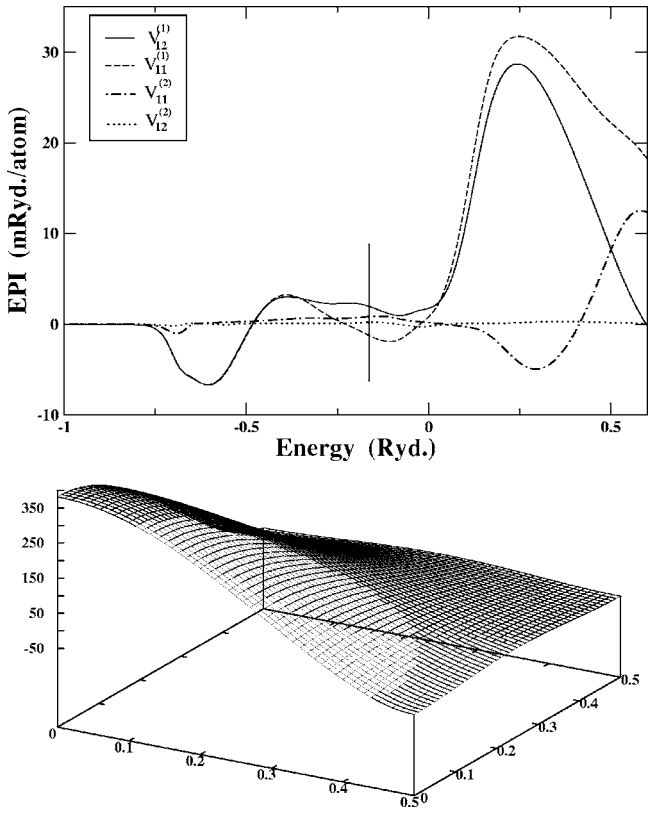

FIG. 5. Effective potentials in real space (top panel) and the Fourier transform evaluated in $k_z=0$ plane (bottom panel) for hcp $Ti_{75}Al_{25}$ alloy. Vertical line in the top panel marks the Fermi energy.

We note that for $Ti_{75}Al_{25}$, the fcc-based calculation gives $L1_2$ as the ordered structure, while hcp-based calculation shows DO_{19} to be the ordered structure—a conclusion reached by two independent computations. With the correspondence between $L1_2$ and DO_{19} of fcc and hcp cases, this gives further confirmation of validity of our calculation.

ACKNOWLEDGMENTS

One of the authors (A.A.) would like to thank the Council of Scientific and Industrial Research, India and T.S.-D. thanks DST for assistance through Swarnajayanti Fellowship. G.P.D acknowledges DMRL for support.

[1] P. Blaha, K. Schwarz, and P. H. Dederichs, Phys. Rev. B **38**, 9368 (1988).
[2] T. Hong, T. J. Watson-Yang, A. J. Freeman, T. Oguchi, and Jian-Hua Xu, Phys. Rev. B **41**, 12462 (1990).
[3] T. Hong, T. J. Watson-Yang, X. Q. Guo, A. J. Freeman, T. Oguchi, and Jian-Hua Xu, Phys. Rev. B **43**, 1940 (1991).
[4] Q. M. Hu, R. Yang, D. S. Xu, Y. L. Hao, D. Li, and W. T. Wu, Phys. Rev. B **68**, 054102 (2003).
[5] O. Jepsen, O. K. Andersen, and A. R. Mackintosh, Phys. Rev. B **12**, 3084 (1975).
[6] J. R. Chelikowksi, C. T. Chan, and S. G. Louie, Phys. Rev. B **34**, 6656 (1986).
[7] J. Kudrnovsky, V. Drchal, and J. Masek, Phys. Rev. B **35**, 2487 (1987).
[8] J. Kudrnovsky, V. Drchal, M. Sob, and O. Jepsen, Phys. Rev. B **41**, 10459 (1990).
[9] J. Kudrnovsky, V. Drchal, M. Sob, and O. Jepsen, Phys. Rev. B **43**, 4622 (1991).
[10] D. Shin, R. Arroyave, Zi-Kui Liu, and A. Van de Walle, Phys. Rev. B **74**, 024204 (2006).
[11] T. Saha, I. Dasgupta, and A. Mookerjee, J. Phys.: Condens. Matter **6**, L245 (1995); T. Saha and A. Mookerjee, *ibid.* **8**, 2915 (1996).
[12] T. Saha and A. Mookerjee, J. Phys.: Condens. Matter **8**, 2915 (1996).
[13] T. Saha, I. Dasgupta, and A. Mookerjee, Phys. Rev. B **50**, 13267 (1994).
[14] F. Ducastelle and F. Gautier, J. Phys. F: Met. Phys. **6**, 2039 (1976).
[15] A. Gonis and J. W. Garland, Phys. Rev. B **16**, 2424 (1977).
[16] H. Dreysse, A. Berera, L. T. Wille, and D. de Fontaine, Phys. Rev. B **39**, 2442 (1989); C. Wolverton, G. Ceder, D. de Fontaine, and H. Dreysse, *ibid.* **48**, 726 (1993).
[17] A. Gonis, X. G. Zhang, A. J. Freeman, P. Turchi, G. M. Stocks, and D. M. Nicholson, Phys. Rev. B **36**, 4630 (1987).
[18] N. R. Burke, Surf. Sci. **58**, 349 (1976).
[19] T. Saha, Ph.D. thesis, Jadavpur University, 1995.
[20] D. Paudyal, T. Saha-Dasgupta, and A. Mookerjee, J. Phys.: Condens. Matter **15**, 1029 (2003).
[21] D. Banerjee, Prog. Mater. Sci. **42**, 135 (1997).
[22] A. Mookerjee, J. Phys. C **6**, L205 (1973).
[23] R Haydock, Solid State Phys. **35**, 216 (1980).
[24] N. Beer and D. G. Pettifor, in *Electronic Structure of Complex Systems*, edited by P. Phariseau and W. M. Tammerman (Plenum, New York, 1984), p. 769.
[25] V. Heine, *Solid State Physics* (Academic, New York, 1988), Vol. 35.
[26] A. G. Khachaturian, Prog. Mater. Sci. **22**, 1 (1978).
[27] F. Ducastelle, *Order and Phase Stability in Alloys* (Elsevier Science, New York, 1991).
[28] K. K. Saha, T. Saha-Dasgupta, A. Mookerjee, and I. Dasgupta, J. Phys.: Condens. Matter **16**, 1409 (2004).
[29] S. Ghosh, N. Das, and A. Mookerjee, Mod. Phys. Lett. B **21**, 723 (1999).
[30] Atisdipankar Chakrabarti and A. Mookerjee, Eur. Phys. J. B **44**, 21 (2005).
[31] I. Ohnuma *et al.*, Acta Mater. **48**, 3113 (2000); M. Asta, D. de Fontaine, M. van Schilfgaarde, M. Sluiter, and M. Methfessel, Phys. Rev. B **46**, 5055 (1992).
[32] R. Benedek, A. van de Walle, S. S. A. Gerstl, M. Asta, D. N. Seidman, and C. Woodward, Phys. Rev. B **71**, 094201 (2005).
[33] G. Rubin and A. Finel, J. Phys.: Condens. Matter **5**, 9105 (1993).
[34] M. Asta, D. de Fontaine, M. van Schilfgaarde, M. Sluiter, and M. Methfessel, Phys. Rev. B **46**, 5055 (1992).